Materials Research Express

PAPER

Ferromagnetism in undoped ZnO grown by pulsed laser deposition

Waqar Azeem[1], **Cai-Qin Luo**[1], **Chi Xu**[2], **Shengqiang Zhou**[2], **A Wagner**[3], **M Butterling**[3], **Muhammad Younas**[4] **and Francis Chi-Chung Ling**[1,5]

[1] Department of Physics, The University of Hong Kong, Pokfulam Road, Hong Kong, People's Republic of China
[2] Institute of Ion Beam Physics and Materials Research, Helmholtz-Zentrum Dresden-Rossendorf, Bautzner Landstr. 400, 01328 Dresden, Germany
[3] Institute of Radiation Physics, Helmholtz-Zentrum Dresden-Rossendorf, Bautzner Landstr. 400, 01328 Dresden, Germany
[4] PCG, Physics Division, PINSTECH, PO Nilore, Islamabad 45650, Pakistan
[5] Author to whom any correspondence should be addressed.

E-mail: ccling@hku.hk

OPEN ACCESS

RECEIVED
8 February 2020

REVISED
16 April 2020

ACCEPTED FOR PUBLICATION
23 April 2020

PUBLISHED
4 May 2020

Keywords: ferromagnetism, ZnO, positron annihilation spectroscopy, vacancy cluster, x-ray diffraction

Abstract

Undoped ZnO films grown on sapphire by pulsed laser deposition are magnetic at room temperature. A comprehensive study involving x-ray diffraction, positron annihilation spectroscopy, and superconducting quantum Interference device-vibrating sample magnetometer is performed to study the origin of the observed magnetization. Correlations between the saturation magnetization, $V_{Zn}-2V_O$ concentration and surface to volume ratio of the grain found experimentally show that the magnetization is associated with the vacancy cluster and probably $V_{Zn}-2V_O$ residing on the grain surface.

Introduction

Since the theoretical prediction of room temperature (RT) ferromagnetism (FM) of transition metal doped ZnO [1], there were extensive research devoted to study the RT FM in transition metal doped ZnO materials [2, 3]. RT FM was reported in ZnO doped with a variety of transition metals [4], namely Mn [5–10], Co [7, 8, 11–17], Fe [18], and Cu [19–21] etc, and defects played important role in mediating the ferromagnetic coupling [6, 20–22]. However, there were concerns that the measured ferromagnetism was originated from the secondary phase [23]. RT FM was also reported in undoped ZnO materials [24–31], which thus makes ZnO a feasible potential material for spintronic applications [24]. The report of bias voltage controlled FM switching in undoped ZnO multi-layer structure device also reveals the potential magneto-electrical device applications [32, 33]. As compared to transition metal doped ZnO, there were relatively fewer RT FM study in undoped ZnO. The origin of the RT FM of undoped ZnO is still controversial. The RT FM has been associated to the surface of nanoparticle, single crystal and grain boundary materials [24–31], though the exact spices contributing for the FM is not unambiguously known. Tietze *et al* [27] suggested that the RT FM was originated from the dangling electrons on the nanoparticle surface. Many other experimental and theoretical studies reported that vacancy type defects could contribute for the RT FM, thought there was no agreement on the identity of the vacancy. In a hybrid density functional theoretical DFT study, Chakrabarty and Patterson [34] reported that the negatively charged $(V_{Zn}V_O)^-$ divacancy and V_{Zn}^- monovacancy are possible origins for RT FM in undoped ZnO. Wang *et al* [35] carried out DFT study in undoped ZnO and found that FM could be originated from the V_{Zn}, arising from the unpaired 2p electrons at the O sites surrounding the V_{Zn}. Their calculation also shows that the V_{Zn} prefers to cluster and resides on the surface of the thin film. Performing density functional theory study, Wu *et al* [36] reported that V_{Zn} in twin grain boundary favours ferromagnetic coupling. The density functional theory within the GGA exchange functional study performed by Lin *et al* [37] showed that V_O could not contribute for net magnetic moment, and the FM was likely originated from the V_O cluster and V_{Zn} complex defects. However, based on the results of experimental and theoretical studies, Sun *et al* [29] suggested that the FM was associated to V_O.

Obtaining the unambiguous origin or the defect microstructure associated with the magnetization observed in undoped ZnO is not easy. A comprehensive study on the correlation between the magnetic property and the stoichiometry of Zn and O during growth could offer the stoichiometric information of the defect associated with the observed magnetization. PAS is probe selectively sensitive to defect containing V_{Zn} which can offer information of the microstructure of the defect [38–40]. The Doppler broadening of the annihilation radiation (which is characterized by the S-parameter) originated from the incident positron and the electron around the defect can reveal the electronic momentum around the defect. The S-parameter depends on the defect microstructure, and for defect having the same microstructure an increase of S-parameter implies a higher defect concentration. Khalid *et al* [26] observed correlation between the magnetization and the S-parameter of the PLD grown undoped ZnO samples grown with different nitrogen pressure, and suggested that Zn vacancy is probably responsible for the magnetic order. However, the S-parameter is a combined effect of the defect microstructure and concentration, and solely the S-parameter study cannot be used to reveal the microstructure of the defect.

In the present study, the undoped ZnO films grown by PLD are all magnetic at room temperature. To study the origin of the magnetization of these samples, a comprehensive approach is adopted. x-ray diffraction (XRD) study is conducted to study the crystalline quality of the film and also the grain surface area to grain volume ratio s_{GB}. PAS study was carried out to reveal the origin of the RT FM. As compared to the PAS study in Khalid *et al* [26] for which the S-parameter approach is adopted, the coincidence Doppler broadening approach is used in the present study, in which the defect microstructure of the involved defect can be identified while comparing the experimental spectrum with the theoretical simulation. The magnetic properties of the samples were studied by the Superconducting Quantum Interference Device-Vibrating sample Magnetometer (SQUID) measurement.

Experimental

The undoped ZnO films were grown on c-plane sapphire substrate using the PLD method, whereas laser pulse with wavelength, energy, spot fluence, and repetition rate of respectively 248 nm, 300 mJ, 7.4 Jcm^{-2} and 2 Hz from a krypton fluoride (KrF) excimer laser (COMPexPro 102 by Coherent Inc.) was used to ablate the ZnO ceramic (purity of 99.999%). The background pressure was 10^{-4} mbar. The samples were grown on the c-sapphire substrate with different oxygen pressures $P(O_2)$ of 0 Pa, 1 Pa and 3 Pa for the fixed growth time of 3 h. This method of growth yields undoped ZnO films with the polarity of O-face [41]. The annealing was carried out in Ar atmosphere for a period of 45 min.

The film thickness was determined by inspecting the sample cross section using the scanning electron microscope (JOEL JSM-7001F). The XRD measurement was conducted using the Bruker D8 Advance. The magnetic measurement was conducted using the Quantum Design SQUID with a sensitivity of 10^{-7} emu. The PAS study was conducted using a monoenergetic positron beam with positron energy varying up to 30 keV. The annihilation gamma energy spectra of the annihilation photons were detected by a high purity Ge (HPGe) detector and the corresponding nuclear electronic system which had an energy resolution of 1.1 keV for the 514 keV gamma radiation peak. The coincidence Doppler broadening of the annihilation radiation lineshape was monitored by the S-parameter and W-parameter, respectively defined as the ratios of the count of the central window (511.00 $\pm$ 0.76 keV) and the ratio of the counts of the wings (511.00 $\pm$ 3.4 keV and 511.00 $\pm$ 6.8 keV) divided by the total spectrum count.

Results

The area and the thicknesses of ZnO films (determined by the cross sectional SEM images) are tabulated in table 1. The film thickness was ~240 nm and ~330 nm for the films grown without and with oxygen respectively. XRD study was performed on the ZnO samples grown with $P(O_2) = 0$, 1 and 3 Pa (Samples A-0Pa, A-1Pa and A-3Pa). The XRD spectrum of the as-grown undoped ZnO films grown with $P(O_2) = 0$ Pa (i.e. A-0Pa) is shown in figure 1(a) with the intensity shown in log scale, which shows that the film has wurtzite structure with (002) as the preferential orientation. Although another ZnO (100) peak is also identified, its intensity is much lower (more than 200 times) than the ZnO (002) peak. The other samples grown with different $P(O_2)$'s have similar XRD pattern. Figure 1(b) shows the ZnO (002) peak of the spectra for the samples, with peak position increasing from 34.47° to 34.57° while $P(O_2)$ increases from 0 Pa to 3 Pa. This shifting to high angle (and so does the decrease in lattice constant) has been attributed to the increase of V_{Zn} (or V_{Zn}-related defect indeed) concentration by Khalid *et al* [26]. The positions and full width at half maximum (FWHM) of the (002) peaks for the samples grown with different $P(O_2)$ are tabulated in table 1. The lattice constant c is calculated by $c = l\lambda/2 \sin\theta$, where l is the Miller indices, λ is the wavelength of incident x-ray and θ is the diffracted angle of

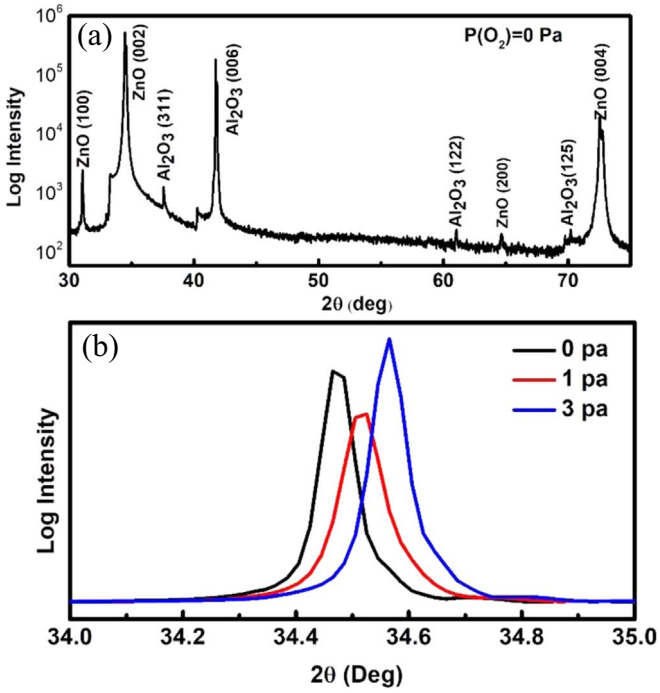

Figure 1. (a) Shows the XRD spectrum of the undoped ZnO sample grown without oxygen; (b) shows the ZnO (002) peaks for the samples grown with different oxygen pressures.

Table 1. Tabulates the film thicknesses, the peak positions and FWHM's of the ZnO (002) peaks, the grain sizes, the grain surface to volume ratio S_{GB}, the lattice constants and the magnetic moments M_S of the undoped ZnO films with different oxygen pressures $P(O_2)$.

PO_2 (Pa)	Film thickness (nm)	Area (cm^2)	Peak position	FWHM (Deg)	Grain size (nm)	$S_{GB} = 1.63/D$ (m^{-1})	Lattice constant c (A°)	M_S emu/g
0	240	0.45	34.47°	0.1688	50.05	3.3×10^7	5.190	0.108
1	330	0.32	34.51°	0.1759	46.82	3.5×10^7	5.188	0.114
3	327	0.37	34.57°	0.1839	45.36	3.6×10^7	5.186	0.119

the (002) peak. Grain size of the thin films is calculated by the Scherer's equation: $D = 0.9\lambda/\beta \cos\theta$, where β is the FWHM. The ratio of grain boundary area to volume (s_{GB}) is calculated by $s_{GB} = 1.65/D$, where D is the mean grain size [28]. The thus calculated values of lattice constant, grain size and s_{GB} for the samples grown with the different $P(O_2)$ are also tabulated in table 1.

The (W,S) parameter plot of the CDB study for the as-grown and 750 °C annealed ZnO samples grown with different $P(O_2)$'s are shown in figure 2. The experimental error bars ΔW and ΔS are included in the figure. The resultant S-parameter (and also the resultant W parameter) is given by $S = f_b S_b + \sum_i f_{d,i} S_{d,i}$, where f_b and f_{di} are respectively the fractions of positron annihilating in the delocalized bulk state and the i-th vacancy states, and S_b and S_{di} are respectively the corresponding characteristic S-parameter [38–40]. If a single type of defect exists, it then yields $(S - S_b)/(W - W_b) = (S_d - S_b)/(W_d - W_b)$, implying that the W-S plot is a stragiht line and the slope is the fingerpring of the vacancy whereas the S-parameter is proportional to the defect concentration [38–40]. The experimental (W,S) parameter data of a ZnO single crystal was also measured and included in figure 2. The positron lifetime spectrum of this ZnO single crystal is well fitted by a single lifetime component of 166 ps, showing that this sample is close to defect-free. All the (W,S) data of the other samples are normalized against those of the ZnO single crystal. It is observed from figure 2 that all the (W,S) data points of the as-grown and 750 °C annealed ZnO samples grown with different oxygen pressures visually lays on a straight line. Linear regression of these data points yields an adjusted R square of 0.99, indicating a very good straight-line fitting to the corresponding data (see the fitted line in the figure). It is thus concluded that the same type of V_{Zn} contained defect exists in these ZnO samples. For the same type of V_{Zn}-related defect, the S-parameter increases (and W-parameter decreases) with the increasing defect concentration. The moving down of the W-S data in figure 2 with increasing $P(O_2)$ implies that the concentration of this V_{Zn}-related defect increases with increasing $P(O_2)$.

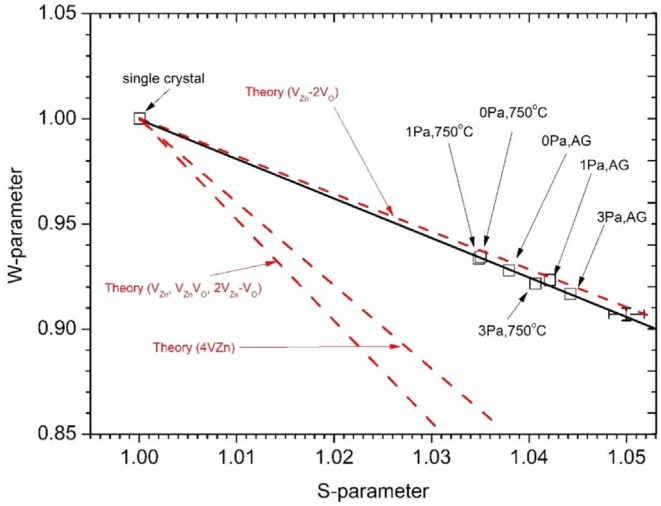

Figure 2. Shows the W-S parameter plot for the undoped as-grown and 750 °C annealed ZnO thin films grown with different oxygen pressures of 0 Pa, 1 Pa and 3 Pa. The W-S data of the ZnO single crystal (which is close to defect free) is also included for reference. The black line is the fitted line of the W-S data of the samples. The red dashed lines are the theoretical characteristic W-S lines for the different V_{Zn}-related defects depicted in reference [22]. The experimental errors of ΔW and ΔS are included in the plot.

For the samples grown with the same $P(O_2)$, the W-S data moves up after annealing at 750 °C, implying the reduction of the defect concentration upon the annealing.

It would be worthy to explore the microstructure of this V_{Zn}-related defect found in these samples. Makkonen *et al* [42] carried out theoretical study on the Doppler broadening of annihilation gamma radiation coming from the V_{Zn}-related defects in ZnO. Their W-S characteristic straight line of V_{Zn} monovacancy and $4V_{Zn}$ vacancy cluster are included in figure 2. It is also found the W-S characteristic straight lines of $V_{Zn}V_O$ and $2V_{Zn}-V_O$ is very close to that of V_{Zn}, and beyond the resolution of the Doppler broadening technique. The vacancy clusters $V_{Zn}-2V_O$ is also studied and its characteristic straight line is shown in figure 2. It is noticed that the characteristic straight line for the defect as found in the current ZnO samples is very close to the theoretical straight lines of the $V_{Zn}-2V_O$ and clearly distinguishable from the other theoretical W-S lines. It is thus plausible to infer that the $V_{Zn}-2V_O$ is the single type V_{Zn}-related defect dominated in these ZnO samples.

Magnetic study was carried out on the as-grown ZnO samples grown with different $P(O_2)$'s (0 Pa, 1 Pa and 3 Pa) which is dominated by $V_{Zn}-2V_O$. The M-H curves of the samples normalized against the film volume (in unit of emu cm^{-1}) are shown in figure 3, and the corresponding magnetization are tabulated in table 1. One of the measurements is shown in the insert low right hand corner of figure 3 in emu without normalization. Hysteresis loop is revealed for all the three samples, though the hysteresis is small. Their saturated magnetization (M_s) are tabulated in table 1, for which the M_S increases from 0.108 to 0.119 emu g^{-1} while $P(O_2)$ increases from 0 Pa to 3 Pa. The coercivities H_C of the 0Pa, 1Pa and 3Pa samples are respectively 119 Oe, 99 Oe and 84 Oe, while their remanences are 0.0148 emu g^{-1}, 0.0129 emu g^{-1} and 0.0118 emu/g. The experimental saturated magnetization of undoped ZnO observed from previous literatures diverges over a wide range, say 0.2 emu g^{-1} for ZnO nanowire [31], and ~0.01 emu g^{-1} for PLD grown ZnO film on sapphire [26]. The saturated magnetization observed in the present study is within the range reported in the literatures of undoped ZnO film grown by PLD. Note that we have also carefully checked the Al_2O_3 substrates used for growing ZnO films. As shown in the inset to figure 3 (the upper left-hand corner), the field-dependent magnetization of the Al_2O_3 substrate shows a linear diamagnetic behavior, but the ZnO film shows a clear deviation from the linear behavior due to the ferromagnetic component.

It is worthy to explore the temperature dependence of the magnetic properties, and the correlation between the saturated magnetization, $V_{Zn}-2V_O$ abundance and surface to volume ratio of the grain. Figure 4(a) shows the zero field cooling (ZFC) and field cooling (FC) temperature dependent magnetization for the as-grown sample grown with $P(O_2) = 0$ Pa. To perform the measurements, the sample was cooled down from room temperature to 5 K. Then a field of 100 Oe was applied. The ZFC curve was measured during warming up. The FC curve was measured after the sample being cooled down from room temperature to 5 K under a field of 10000 Oe. Then the field was set to 100 Oe. The FC magnetization was also recorded during warming up. The irreversibility between ZFC/FC curves would be due to the ferromagnetic component, which persists well above room temperature in this sample. Figure 4(b) shows the temperature dependent magnetization for this sample measured under 10000 Oe which insures the saturation. Below 50 K, the saturation magnetization shows a fast drop with increasing temperature, which might be due to a small paramagnetic component arising from

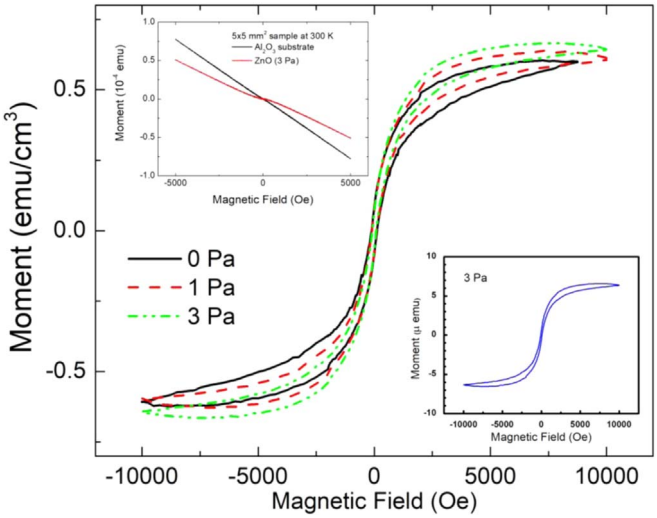

Figure 3. Shows the magnetic moment against the magnetic field in the unit of emu cm^{-3} for the undoped ZnO samples grown with different oxygen pressures $P(O_2)$. These M-H curves in emu cm^{-3} are normalized against the film volume from the M-H curves obtained from the SQUID measurement (like the one of the $P(O_2) = 3$ Pa sample shown in the lower right insert) after diamagnetism subtraction. The left upper insert to figure 3 shows the as-measured field-dependent magnetization at 300 K of a ZnO film and a Al_2O_3 substrate with the same size. The Al_2O_3 substrate shows a linear diamagnetic behavior, but the ZnO film shows a clear deviation from the linear behavior due to the ferromagnetic component.

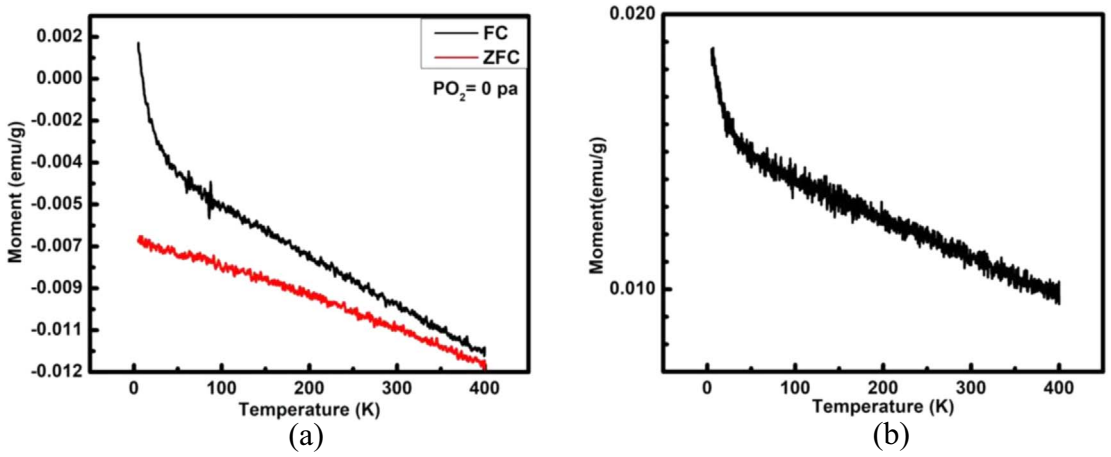

Figure 4. (a) Shows the temperature dependent magnetization after zero field cooling (ZFC) and field cooling (FC) for the as-grown ZnO sample grown with $P(O) = 0$ Pa. The details of measurement is given in the text; (b) shows the temperature dependent magnetization for the same sample measured under 10000 Oe which insures the saturation.

uncoupled defects. Above 50 K, the saturation magnetization shows mild decrease with increasing temperature, indicating the Curie temperature for the ferromagnetic component is well above room temperature.

The fraction of positron annihilating at $V_{Zn}-2V_O$ (f_{defect}) is related to its concentration and can be found by $f_{defect} = (S - S_b)/(S_d - S_b)$ if single type of the vacancy type defect exists. Figure 5 summarizes the saturated magnetization M_S, fraction of positron annihilating at $V_{Zn}-2V_O$, and the grain surface area to volume ratio S_{GB} as a function of $P(O_2)$ for the as-grown samples grown with different $P(O_2)$'s. While $P(O_2)$ increases from 0 Pa to 3 Pa, the corresponding M_S, S_{GB} and f_{defect} increase from 0.108 emu g^{-1} to 0.119 emu g^{-1}, 3.3×10^7 m^{-1} to 3.6×10^7 m^{-1}, and 0.33 to 0.37 respectively. These correspond to the fractional changes of $\Delta M_S/M_S \sim 10\%$, $\Delta s_{GB}/s_{GB} \sim 9\%$ and $\Delta f_{defect}/f_{defect} \sim 12\%$. These fractional changes are close, thus suggesting that the correlations between the saturation magnetization, grain boundary surface and the $V_{Zn}-2V_O$ concentration. This implies that the observed RT FM in the current undoped ZnO films is associated with the $V_{Zn}-2V_O$ residing in the vicinity of the grain boundary.

Khalid *et al*'s [26] previous experimental magnetic studies on the PLD grown undoped ZnO films correlated with results of PAS using the S-parameter approach revealed that the magnetization is associated with defect or defect complex consisting of V_{Zn}. As compared to the present CDBS approach which identified defect structure

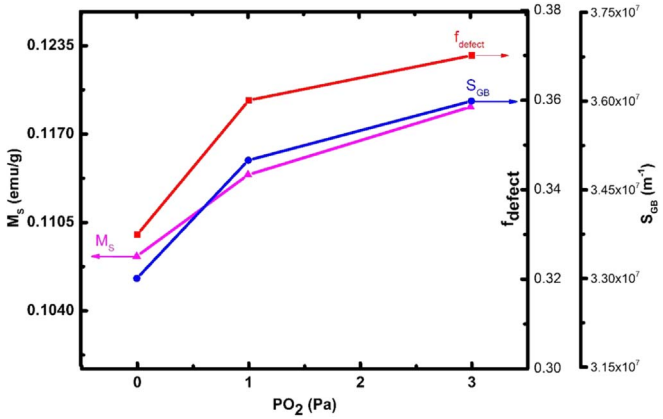

Figure 5. Shows the magnetic moment M_S, the fraction of positron annihilating at the defect site f_{defect}, and the ratio of grain surface to volume S_{GB} against the growth oxygen pressure $P(O_2)$ for the as-grown undoped ZnO.

of $V_{Zn}-2V_O$ in the ZnO samples, the S-parameter approach is not able to offer the microstructure of the V_{Zn}-related defect complex or vacancy cluster. Though there were theoretical magnetic studies on the $V_{Zn}V_O$ divacancy, monovacancies of V_{Zn} and V_O [29, 34–37], no theoretical magnetic study has been reported on the vacancy cluster $V_{Zn}-2V_O$. The magnetic properties of $V_{Zn}-2V_O$ (like net magnetic moment and magnetic state stability) is not known. Nevertheless, it can be concluded that the observed magnetization of the undoped as-grown O-polar ZnO samples grown by PLD is correlated with the $V_{Zn}-2V_O$ residing on the grain surface.

Conclusion

The undoped ZnO samples grown by PLD at oxygen pressures of 0 Pa, 1Pa and 3 Pa are magnetic at RT and the hysteresis is small. The dominating V_{Zn}-related defect in these samples is the $V_{Zn}-2V_O$ vacancy cluster. Experimental correlations between the magnetization, the abundance of $V_{Zn}-2V_O$ and the surface to volume ratio of the grain unambiguously show that the magnetization is associated with the $V_{Zn}-2V_O$ residing on the grain surface. However, the physics of how the magnetism is arisen from this defect is not known and requires theoretical study.

Acknowledgments

This work was financially supported by the HKSAR RGC GRF (17302115).

ORCID iDs

Cai-Qin Luo https://orcid.org/0000-0003-4368-0627
Chi Xu https://orcid.org/0000-0002-1299-7667
Shengqiang Zhou https://orcid.org/0000-0002-4885-799X
Francis Chi-Chung Ling https://orcid.org/0000-0003-4757-1065

References

[1] Sato K and Katayama-Yoshida H 2000 *Japan. J. Appl. Phys.* **39** L555
[2] Liu F Y C and Morkoc H 2005 *J. Mater. Sci., Mater. Electron.* **16** 555
[3] Pearton S J, Heo W H, Ivill M, Norton D P and Steiner T 2004 *Semicond. Sci. Technol.* **19** R59
[4] Opel M *et al* 2014 *Physica Status Solidi (b)* **251** 1700
[5] Kundaliya D C *et al* 2004 *Nat. Mater.* **3** 709
[6] Liu W, Tang X and Tang Z 2013 *J. Appl. Phys.* **114** 123911
[7] Kittilstved K R, Liu W K and Gamelin D R 2006 *Nat. Mater.* **5** 291
[8] Di Trolio A, Larciprete R, Turchini S and Zema N 2010 *Appl. Phys. Lett.* **97** 052505
[9] Di Trolio A, Veroli C, Testa A M and Fiorani D 2009 *Superlattices Microstruct.* **46** 101
[10] Kittilstved K R and Gamelin D R 2005 *Journal of American Chemical Society* **127** 5292
[11] Ueda K, Tabata H and Kawai T 2001 *Appl. Phys. Lett.* **79** 988
[12] Ramachandran S, Tiwari A and Narayan J 2004 *Appl. Phys. Lett.* **84** 5255

[13] Chambers S A, Droubay T C, Wang C M, Rosso K M, Heald S M, Schwartz D A, Kittilstved K R and Gamelin D R 2006 *Mater. Today* **9** 28
[14] Gacic M, Jakob G, Herbort C, Adrian H, Tietze T, Brück S and Goering E 2007 *Physical Review* B **75** 205206
[15] Li X-L, Wang Z-L, Qin X-F, Wu H-S, Xu X-H and Gehring G A 2008 *J. Appl. Phys.* **103** 023911
[16] Schwartz D A and Gamelin D R 2004 *Adv. Mater.* **16** 2115
[17] Di Trolio A, Alippi P, Ciatto G, Scavia G, Valentini M and Amore Bonapasta A 2015 *Journal of Materials Chemistry* C **3** 10188
[18] Karmakar D, Mandal S K, Kadam R M, Paulose P L, Rajarajan A K, Nath T K, Das A K, Dasgupta I and Das G P 2007 *Physical Review* B **75** 144404
[19] Buchholz D B, Chang R P H, Song J Y and Ketterson J B 2005 *Appl. Phys. Lett.* **87** 082504
[20] Herng T S *et al* 2010 *Phys. Rev. Lett.* **105** 207201
[21] Tian Y, Li Y, He M, Putra I A, Peng H, Yao B, Cheong S A and Wu T 2011 *Appl. Phys. Lett.* **98** 162503
[22] Coey J M, Venkatesan M and Fitzgerald C B 2005 *Nat. Mater.* **4** 173
[23] Zhou S, Potzger K, von Borany J, Grötzschel R, Skorupa W, Helm M and Fassbender J 2008 *Physical Review* B **77** 035209
[24] Qi B, Ólafsson S and Gíslason H P 2017 *Prog. Mater Sci.* **90** 45
[25] Hong N H, Sakai J and Brizé V 2007 *J. Phys. Condens. Matter* **19** 036219
[26] Khalid M *et al* 2009 *Physical Review* B **80** 035331
[27] Tietze T *et al* 2015 *Sci. Rep.* **5** 8871
[28] Straumal B B, Mazilkin A A, Protasova S G, Myatiev A A, Straumal P B, Schütz G, van Aken P A, Goering E and Baretzky B 2009 *Physical Review* B **79** 205206
[29] Sun Y, Zong Y, Feng J, Li X, Yan F, Lan Y, Zhang L, Ren Z and Zheng X 2018 *J. Alloys Compd.* **739** 1080
[30] Zhang H, Li W, Qin G, Ruan H, Wang D, Wang J, Kong C, Wu F and Fang L 2019 *Solid State Commun.* **292** 36
[31] Yi J B, Pan H, Lin J Y, Ding J, Feng Y P, Thongmee S, Liu T, Gong H and Wang L 2008 *Adv. Mater.* **20** 1170
[32] Li S S, Chuang R W, Su Y K and Hu Y M 2016 *Appl. Phys. Lett.* **109** 252103
[33] Younas M *et al* 2017 *ACS Omega* **2** 8810
[34] Chakrabarty A and Patterson C H 2011 *Physical Review* B **84** 054441
[35] Wang Q, Sun Q, Chen G, Kawazoe Y and Jena P 2008 *Physical Review* B **77** 205411
[36] Wu J and Tang X 2019 *Mater. Res. Express* **6** 1150d4
[37] Lin Q L, Li G P, Xu N N, Liu H, D J E and Wang C L 2019 *J. Chem. Phys.* **150** 094704
[38] Coleman P 2000 *Positron Beams and Their Applications* (Singapore: World Scientific)
[39] Krause-Rehberg H S L R 1999 *Positron Annihilation in Semiconductors: Defect Studies* (Berlin: Springer)
[40] Tuomisto F and Makkonen I 2013 *Rev. Mod. Phys.* **85** 1583
[41] Luo C-Q *et al* 2019 *Appl. Surf. Sci.* **483** 1129
[42] Makkonen I, Korhonen E, Prozheeva V and Tuomisto F 2016 *Journal of Physics. Condensed Matter : An Institute of Physics Journal* **28** 224002